ORIGINAL ARTICLE

CrossMark

Green synthesis of magnetite nanoparticles using aqueous pod extract of *Dolichos lablab* L for an efficient adsorption of crystal violet

K. Basavaiah[1] · Mebrahtu Hagos Kahsay[1,2] · Dharmasoth RamaDevi[3]

Abstract

We report, an aqueous pod extract of *Dolichos lablab* L. mediated synthesis of magnetite nanoparticles (Fe_3O_4 NPs) for an efficient adsorption of organic dye pollutant from contaminated water. The Fe_3O_4 NPs were capped and stabilized with phytoconstituents of *D. lablab* L. The product Fe_3O_4 NPs was characterized by range of instrumental facilities such as Ultraviolet–visible spectroscopy, Fourier transform infrared spectroscopy, FT-Raman spectroscopy, X-ray diffraction, Field emission scanning electron microscopy, Energy dispersive X-ray spectroscopy, Transmission electron microscopy, vibrating sample magnetometer, and thermogravimetric analysis. The synthesized 12.5 nm spherical shaped Fe_3O_4 NPs were used as adsorbent for elimination of crystal violet (CV) from contaminated water. It is found that the dye removal efficiency of Fe_3O_4 NPs was critically depends on pH of the reaction medium and dosage of Fe_3O_4 NPs. Adsorption data were analyzed using Langmuir, Freundlich, and Temkin isotherms as well as pseudo-first-order and pseudo-second-order kinetic models. The overall outcome of adsorption best fitted to Langmuir and psepseudo-second-order with their corresponding correlation coefficients of ($R^2 = 0.996$) and ($R^2 = 0.977$), respectively The biomolecules capped can act as a valuable adsorbent for removal of pollutant organic dyes from industrial outflow.

Keywords Adsorption · Crystal violet · Fe_3O_4 NPs · *Dolichos lablab* pod · Green synthesis · Pseudo-second-order

1 Introduction

During the last two decades, magnetite nanoparticles (Fe_3O_4 NPs) have attracted considerable attention to researchers due to their unique chemical and physical properties and many technological applications. Fe_3O_4 NPs have been exclusively studied owing to their special properties and potential technological applications such as magnetic storage media [1], catalyst for dye removal [2], adsorbent [3], magnetic resonance imaging [4, 5], drug delivery [6], ferrofluids [7], biosensors [8], hyperthermia

✉ K. Basavaiah
klbasu@gmail.com

1 Department of Inorganic and Analytical Chemistry, Andhra University, Visakhapatnam 530003, India

2 Faculty of Natural and Computational Sciences, Woldia University, 400 Woldia, Ethiopia

3 A.U College of Pharmaceutical Sciences, Andhra University, Visakhapatnam 530003, India

treatment of cancer [9–11] and organic synthesis [12]. Fe_3O_4 NPs have been exclusively employed for wastewater treatment due to their dynamic morphology, desired size, magnetic property and value saturation magnetization value [13]. Among all water treatment techniques, the adsorption process is one of the most widely used owing to a benefit of high adsorption efficiency and non toxic by products release into treated water [14].

Various synthesis methods mostly physical and chemical methods have been reported for Fe_3O_4 NPs such as, redox-based hydrothermal method [15], solvothermal synthesis [16], co-precipitation [17], flame spray synthesis [18], sol-gel method [19], electrochemical processes [20], high energy ball milling [21], and sonochemical synthesis [22]. However, physical and chemical methods bring argument to environmental and biological risks on account of the use of toxic precursors, capping agents, solvents and toxic reducing agents especially hydrazine [23], sodium borohydride ($NaBH_4$), carbon monoxide (CO) [24], and dimethyl formamide (DMF) [25] during synthesis of Fe_3O_4 NPs [26]. Therefore, the researchers are profoundly motivated to green synthesis of Fe_3O_4 NPs via nature-friendly, and inexpensive approach for environmental and medical applications.

More recently, green chemistry drew attention to many researchers for synthesis of Fe_3O_4 NPs by using various biological entities such as plants, and microbes (bacteria, fungi, yeasts,

QAPCO · جامعة قطر QATAR UNIVERSITY · ⚫ Springer

and algae) [27–30] as reducing and capping agents. In case of microbe assisted synthesis of nanoparticles, there are several limitations, including tedious purification steps and the difficulty to maintain the microbial culture. However, plant extract mediated synthesis of Fe_3O_4 NPs offers simple and green synthesis approach. Authors have reported synthesis of Fe_3O_4 NPs have been synthesized via plant mediated synthesis using plant extract of *Datura inoxia* [31], *Artemisia annua* [12], carob [32], soya bean sprouts templates, [33], *Sesbania grandiflora* [34], green tea [35], *Vanilla planifolia*, *Cinnamomun verum* [36], *Hordeum vulgare*, *Rumex acetosa* [37], and Sorghum bran [38] as reducing and capping agents

To the best of our knowledge, an aqueous pod extract of *Dolichos lablab* had never been used for synthesis of Fe_3O_4 NPs. In the present study, we report the green synthesis of Fe_3O_4 NPs using an aqueous pod extract of *Dolichos lablab* L as capping and reducing agents. Further, the synthesized Fe_3O_4 NPs was used in water treatment to clear away crystal violet (CV) dye from aqueous solution. The dye removal efficiency by Fe_3O_4 NPs is investigated as a function of dose of Fe_3O_4 NPs, pH, amount of dye, and effect of temperature.

2 Materials and methods

2.1 Materials

All chemicals were analytical grade used without additional refinement. Iron (II) sulfate heptahydrate ($FeSO_4 \cdot 7H_2O$), CV dye and Sodium hydroxide (NaOH) were purchased from Merck, India and Iron (III) chloride hexahydrate ($FeCl_3 \cdot 6H_2O$) from Himedia, India. All aqueous solutions prepared in these experiments were from distilled Milli-Q water. *Dolichos lablab* L was collected from Andhra University, Andhra Pradesh, India. Pocket-sized pH meter from Hanna instruments was used to adjust pH of solutions. Hot Air Oven, Kemi was used to dry washed samples.

2.2 Preparation of aqueous pod extract of *Dolichos lablab* L

Pod layers was separated from the seeds and cut into pieces by plastic knife and shade dried in the laboratory for 22 days. Dried pods were ground into powder using Bajaj (Gx8) mixer grinder. To prepare 1% pod extract of *Dolichos lablab*, 1 g pod powder was poured into 250 mL conical flask containing 100 mL Milli-Q water and heated at 70 °C for 20 min. The plant extract was cooled and filtered with Whatman no. 42 filter paper to produce a yellowish solution. Finally, the filtrate was stored in a refrigerator at 4 °C for further synthesis of Fe_3O_4 NPs.

2.3 Synthesis of magnetite nanoparticles using a pod extract of *Dolichos lablab* L

Fe_3O_4 NPs was synthesized by using ferrous and ferric salts in oxygen free atmosphere at ambient temperature [39]. 2:1 M ratio of $FeCl_3 \cdot 6H_2O$ (1.11 g) and $FeSO_4 \cdot 7H_2O$ (0.556 g) were added into 250 mL round bottomed flask and sonicated for 10 min. Following, the solution was heated at 80 °C while magnetically stirring for the later 10 min. Then, 5 mL pod extract of *Dolichos lablab* and 20 mL of 1 M NaOH were added drop by drop stepwise at 80 °C under constant stirring. The appearance of black precipitate confirmed the successful synthesis of Fe_3O_4 NPs. Finally, the produced nanoparticles were washed with Milli-Q water twice and ethanol by centrifugation at 10000 RPM for 15 min, and dried under vacuum for 12 h.

2.4 Characterization of magnetite nanoparticles

The UV-vis absorption spectra were recorded using a Shimadzu 2450–SHIMADZU spectrometer. Fourier transform-infrared (FTIR) spectra were recorded over the range of 400–4000 cm^{-1} using a SHIMADZU-IR PRESTIGE-2 spectrometer to identify the biomolecules responsible for capping and reducing the Fe_3O_4 NPs. X-ray diffraction (XRD) patterns were recorded by PANalytical X'pert pro diffractometer at 0.02 degree/s scan rate using Cu-kα_1 radiation (1.5406 A^0, 45 kV, 40 mA). The shape, size and morphology of Fe_3O_4 NPs were characterized by transmission electron microscopy (TEM model FEI TECNAI G2 S-Twin) at an accelerating voltage of 200 kV. The morphology of the sample was characterized using field emission scanning electron microscopy (FE-SEM, Zeiss Ultra-60) equipped with X-ray energy dispersive spectroscopy (EDX). The magnetic properties of Fe_3O_4 NPs were measured by using vibrating sample magnetometer (VSM) (Lake Shore Cryotronics, Inc., Idea-VSM, model 7410, USA). The thermal properties of the Fe_3O_4 NPs were analyzed by Nietzsche Thermogravimetric/differential thermal analysis (TGA-derivative TGA) (NETZSCH STA 449 F3 Jupiter). The synthesized nanoparticles (6.934 mg) were placed in a platinum sample pan and heated under an N_2 atmosphere from 38 to 736 °C at a heating rate of 20 °C min^{-1}. Raman spectra was obtained using FT-Raman spectroscopy (Bruker RFS 27, USA) with laser source Nd (YAG 1064 nm) at 2 cm^{-1} resolution. 16 + mW laser power was irradiated on *Dolichos lablab* mediated Fe_3O_4 NPs to collect Raman spectra over the wide range 4000 to 50 cm^{-1}.

2.5 Batch mode adsorption of crystal violet

Batch adsorption experiments were carried out using CV dye adsorbate as a model organic pollutant and synthesized Fe_3O_4 NPs as an adsorbent. In order to investigate the dye removal

efficiency of Fe_3O_4 NPs, 50 mg Fe_3O_4 NPs was used as an adsorbent at various concentrations (5, 10, 15, and 20 ppm) of 50 mL CV solution. The pH of CV solution was maintained using dilute 0.1 M HCl/0.1 M NaOH solutions. Then the container containing both adsorbate and adsorbent was stirred for 200 min and in each 20 min time interval 3 ml sample was collected at a time and absorbance readings were recorded at maximum wavelength (λ_{max} = 586 nm) of CV using UV-vis absorption spectrophotometer. Prior to the absorbance spectrum, both centrifugation and magnetic bars were used to separate the adsorbent from solution. Kinetics of adsorption was investigated by taking sample readings per unit time. Adsorption capacity of CV (q) on the surface of Fe_3O_4 NPs was calculated as Eq. 1.

$$q = (C_o - C_e) \, V/m \qquad (1)$$

Where, 'q' is the amount of dye adsorbed at equilibrium ($mg \cdot g^{-1}$), 'C_o' is initial dye concentration ($mg \cdot L^{-1}$), C_e is the dye concentration at equilibrium ($mg \cdot L^{-1}$), 'V' is the volume of aqueous solution (L) and 'm' is mass of Fe_3O_4 NPs (g).

Similarly, the removal efficiency of CV by Fe_3O_4 NPs was calculated using Eq. 2.

$$\eta \, (\%) = (C_o - C_e)/C_o \times 100 \qquad (2)$$

Where, 'C_o' is initial dye concentration (mg/L), 'C_e' is the dye concentration at equilibrium ($mg \cdot L^{-1}$) and 'η' is removal percent (%). The adsorption isotherm was investigated using Langmuir, Freundlich, and Temkin; whereas kinetics was studied using pseudo-first and pseudo-second-order kinetics models.

3 Results and discussion

3.1 Characterization of Fe_3O_4 NPs using a pod extract of Dolichos lablab L

In this study, Fe_3O_4 NPs was successfully synthesized via green approach at 2:1 M ratio of iron salts (Fe^{3+}/Fe^{2+}) using less costly and environmentally benign aqueous pod extract of Dolichos lablab as reducing and capping agent by co-precipitation. First, salt solution and pod extract of Dolichos lablab were sonicated and heated at 80 °C until a brown colored solution was observed. Then, freshly prepared 1 M NaOH solution was added drop by drop to form black nanoparticles, which indicated the formation of Fe_3O_4 NPs. The simplified proposed synthesis mechanism of Fe_3O_4 NPs using polyphenolic compound such as kievitone as bioactive molecule of Dolichos lablab is depicted in Fig. 1. The qualitative analysis of pod of Dolichos lablab and Fe_3O_4 NPs using UV-vis, FTIR and FT-Raman spectroscopy; confirmed the as synthesized Fe_3O_4 NPs were capped mainly with the OH group containing

phytoconstituents of the pod extract of Dolichos lablab L. The synthesized Fe_3O_4 NPs had magnetic property because they were attracted by external magnetic field using Neodymium disc magnets, Fig. S1†. The phytoconstituents present in an aqueous pod extract of Dolichos lablab L were acted as capping and reducing agent for the formation of Fe_3O_4 NPs. The chemical constituents and compositions of Dolichos lablab (Field Bean) pod using gas chromatographic-mass spectrometric (GC-MS) method are listed in Table S1† [40]. Belachew et al. [41] have reported L-Serine capped Fe_3O_4 NPs for the purpose of removal of Rhodamine B from polluted water using batch adsorption method. We believe that the fatty acid methyl esters (methyl laurate, methyl myristate, methyl stearate, methyl palmitate, and methyl linoleate) may have involved as capping and reducing agents during synthesis of Fe_3O_4 NPs using a pod extract of Dolichos lablab. Methyl stearate has a property of nonionic surfactant, emulsifier and stabilizer [42].

The absorption spectrum of Fe_3O_4 NPs is presented in Fig. 2a. The absorption peak at 285 nm is ascribed to the formation of Fe_3O_4 NPs, which is in good agreement with the literature [25].

The FTIR spectra of pod of Dolichos lablab and Fe_3O_4 NPs are presented in Fig. 2b. The characteristic intense bands for a pod extract of Dolichos lablab were observed at 3314 cm^{-1}, 2929 cm^{-1}, 2360 cm^{-1}, 1643 cm^{-1}, 1546 cm^{-1}, 1396 cm^{-1}, 1049 cm^{-1} were due to O–H stretching, C–H stretching vibration of alkane group, O=C=O stretching, conjugated C=C stretching, primary amide N–H bending, aryl C–N stretching and S=O stretching; respectively. The characteristic bands for Fe_3O_4 NPs were observed at 3415 cm^{-1}, 2360 cm^{-1}, 1723 cm^{-1}, 1604 cm^{-1}, 1359 cm^{-1}, 1117 cm^{-1}, 583 and 410 cm^{-1} were ascribed to O–H stretching of the polyphenolic molecule, O=C=O stretching, C=O stretching, C=C stretching, O–H bending of phenols, C–N stretching and O–Fe–O stretching, respectively [43]; which confirms not only the formation of Fe_3O_4 NPs but also capping of Fe_3O_4 NPs by phytoconstituients present in the aqueous pod extract of Dolichos lablab.

The phase purity of the as prepared Fe_3O_4 NPs was characterized by powder XRD. The XRD patterns of Fe_3O_4 NPs is depicted in Fig. 3. All the diffraction peaks at $2\theta = 30.13°$, 35.54°, 43.19°, 54.12°, 57.21° and 62.76° are indexed to face centred cubic magnetite (JCPDS file No. 89–4319), corresponding to the crystal planes of (220), (311), (400), (422), (333) and (440); respectively. The sharp and intense peaks indicated that the high crystallinity and pure phase Fe_3O_4 NPs. The results are also in agreement with reported synthesis of Fe_3O_4 NPs [32, 44]. The average crystallite size of the synthesized Fe_3O_4 NPs was calculated using the well known Debye–Scherrer formula (Eq. 3) to be 13 nm.

$$D_{(hkl)} = k\lambda/\beta\cos\theta \qquad (3)$$

Fig. 1 A proposed mechanism of Fe$_3$O$_4$ NPs using an aqueous pod extract of *Dolichos lablab* L.
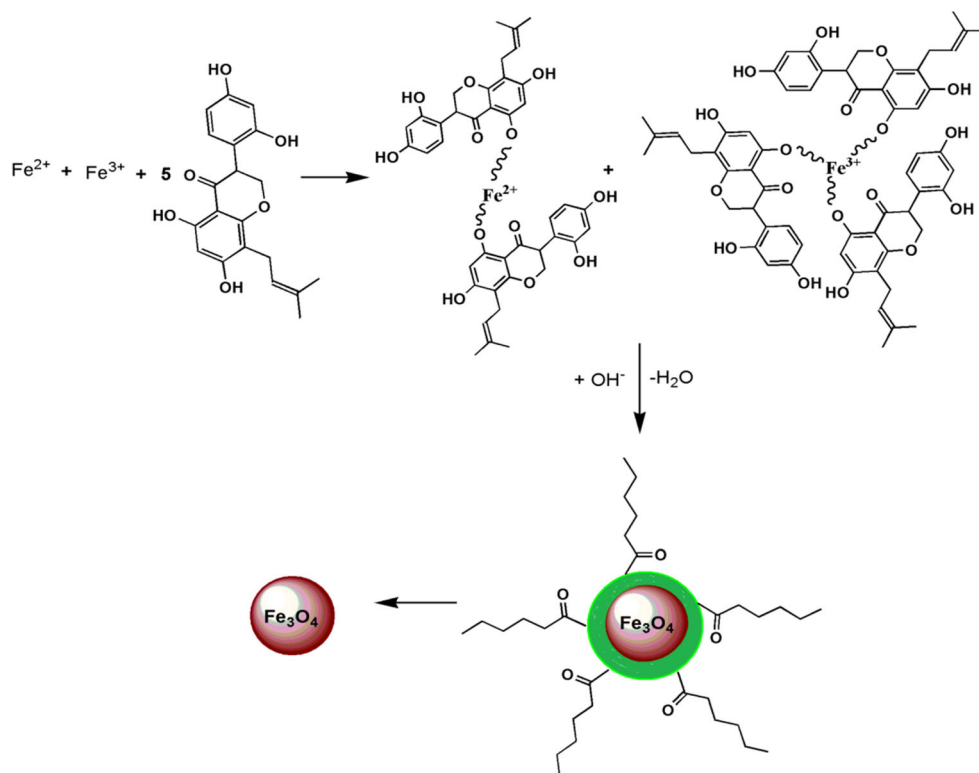
Where, 'D$_{(hkl)}$' is the average crystalline diameter, 'k' is Scherrer constant (0.94), 'λ' is the X-ray wavelength, 'β' is the half width of XRD diffraction line, and 'θ' is the Bragg's angle in degrees.

The surface morphology of the synthesized Fe$_3$O$_4$ NPs was explored by using FE-SEM; Fig. 4 clearly show the spherical shaped Fe$_3$O$_4$ NPs with particle size of 8 to 60 nm. The presence of elemental iron (Fe) and oxygen (O) in EDX spectrum confirmed successful synthesis of Fe$_3$O$_4$ NPs, (Fig. 4d). The elemental composition of Fe and O in Fe$_3$O$_4$ NPs were found to be 31.01 and 68.99% by atomic mass, respectively.

The representative TEM images of Fe$_3$O$_4$ NPs are represented in Fig. 5. TEM results revealed that spherical shaped Fe$_3$O$_4$ NPs with size range of 4 to 30 nm. The SAED patterns confirmed that the polycrystalline nature of as prepared Fe$_3$O$_4$ NPs, (Fig. 5c). The particle size distribution histogram (Fig. 5d) clearly shows Fe$_3$O$_4$ NPs have average particle size of 12.5 nm.

The room temperature magnetization curve of as prepared Fe$_3$O$_4$ NPs is depicted in Fig. 6. The saturation magnetization (Ms) value for Fe$_3$O$_4$ NPs was found to be 31.68 emu/g and which is lower than the bulk counterpart i.e., 92 emu/g [45]. The decrease in 'Ms' value of Fe$_3$O$_4$ NPs could be due to smaller
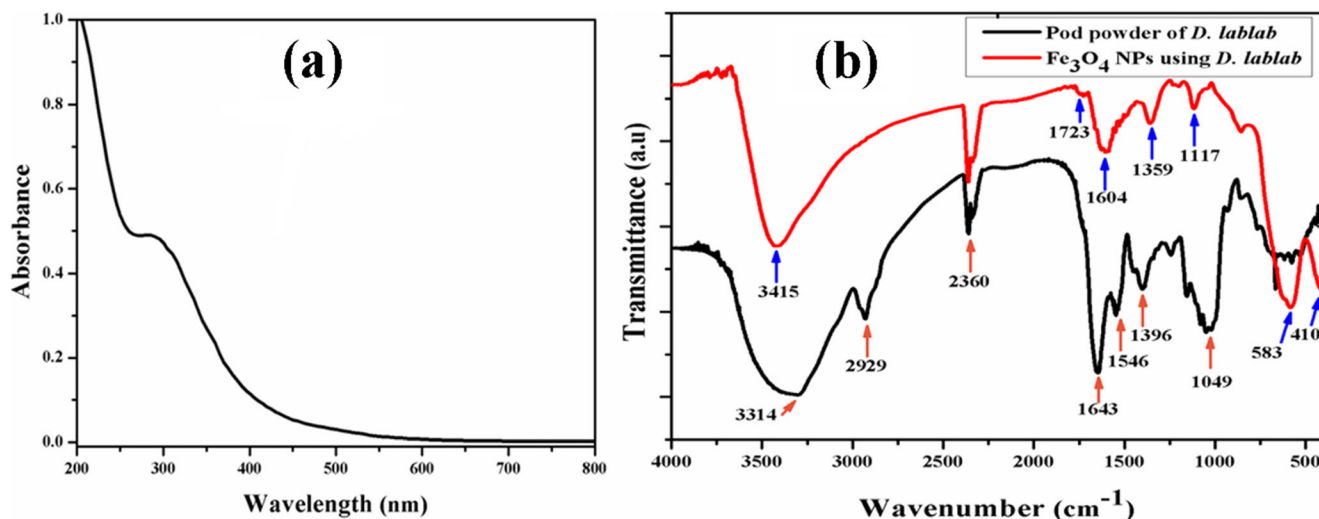

Fig. 2 **a** UV–vis spectra of Fe$_3$O$_4$ NPs, **b** FT-IR spectra of pod of *Dolichos lablab* and Fe$_3$O$_4$ NPs
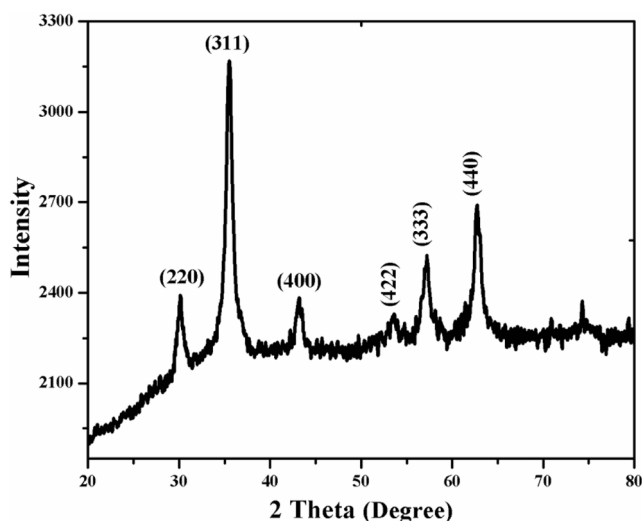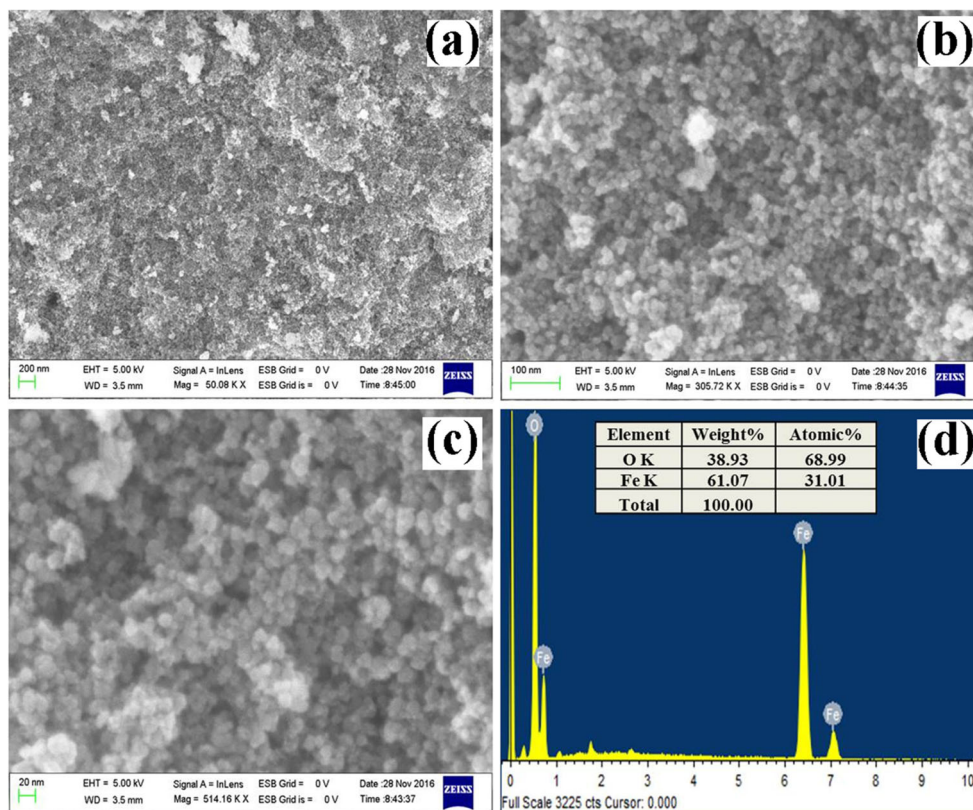
Fig. 3 Powder XRD patterns of Fe_3O_4 NPs

size, or large surface area to volume ratio of the nanoparticles and capping of non-magnetic plant extract on Fe_3O_4 NPs.

Figure 7 shows TGA and derivative TGA of Fe_3O_4 NPs at a rate 20 °C/min under Nitrogen atmosphere. The weight loss below 100 °C and below 267 °C is ascribed due to loss of water and organic components from the surface of Fe_3O_4 NPs. The weight loss between 267 and 300 °C is associated due to loss of biomolecules such as methyl laurate, methyl myristate and methyl stearate fatty acid esters from the surface of Fe_3O_4

NPs. In addition, weight loss at 444 °C may be due to thermal crystal phase transformation from Fe_3O_4 to γ-Fe_2O_3 [46].

FT-Raman spectra of *Dolichos lablab* mediated Fe_3O_4 NPs using using 16 + mW laser power is depicted in Fig. 8. The presence of a shift peak at around 634 cm^{-1} confirms formation of Fe_3O_4 NPs using an aqueous extract of *Dolichos lablab*. In addition, the peak at 3128 cm^{-1} which is broadened and shifted by H-bonding represents the OH group of phenolic compound from the plant extract and is also supported with result in the FTIR spectrum [47]. FT-Raman also confirms the synthesized Fe_3O_4 NPs is capped with the plant extract. Raman spectra of Fe_3O_4 NPs recorded at 0.35 mV after exposure for 7 min showed characteristic peak at 670 cm^{-1} [48].

3.2 Removal of crystal violet from contaminated water

The CV present in the contaminated water is removed by using as prepared Fe_3O_4 NPs. The effect of initial dye concentration, pH, load of Fe_3O_4 NPs and temperature on CV removal efficiency of Fe_3O_4 NPs was investigated.

3.2.1 Effect of initial dye concentration

The effect of initial dye concentration relies on the immediate relation between the concentrations of dye and the porous sites on the surface of Fe_3O_4 NPs. Different initial concentrations of

Fig. 4 **a**–**c** FE-SEM images of Fe_3O_4 NPs at different magnifications and **d** EDX spectrum of Fe_3O_4 NPs

Element	Weight%	Atomic%
O K	38.93	68.99
Fe K	61.07	31.01
Total	100.00	

Fig. 5 **a**–**b** TEM images of Fe_3O_4 NPs, **c** SAED patterns of Fe_3O_4 NPs and **d** Size distribution histogram of Fe_3O_4 NPs
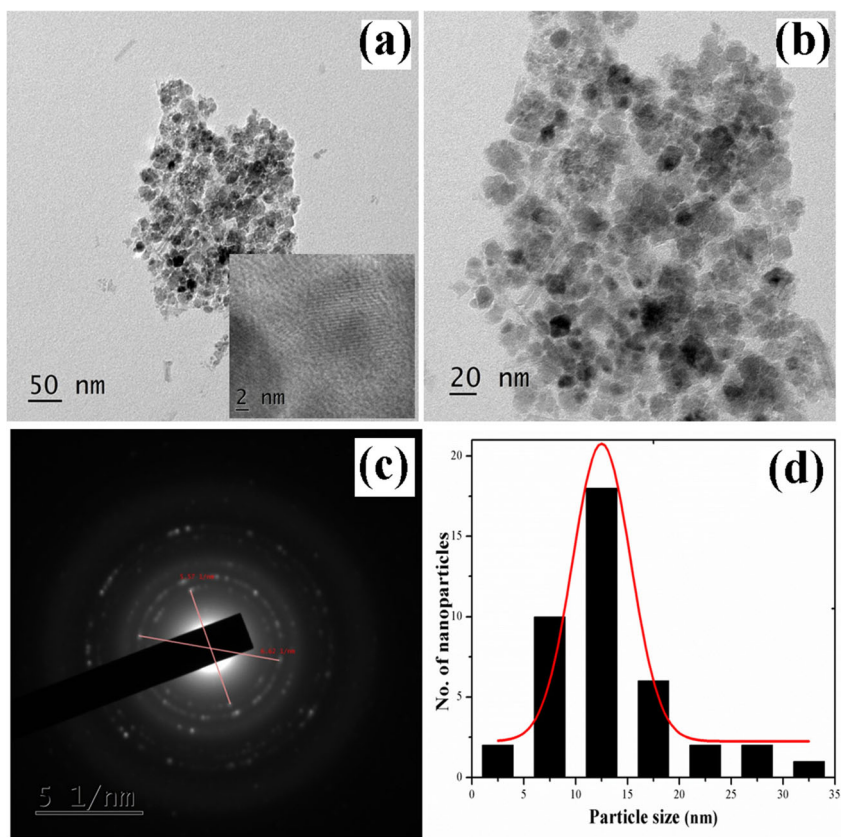
CV dye (5, 10, 15, 20 mg·L^{-1}) were prepared. In 250 mL beaker, 50 mL of the prepared dye solution was added and 50 mg of Fe_3O_4 NPs was added and stirred until equilibrium was established. Then each solution was centrifuged and the amount of dye remained not adsorbed was determined by UV-vis spectrophotometer. The dye removal efficiency was decreased with an increase in the initial dye concentration, which could be due to the saturation of adsorption sites on the Fe_3O_4 NPs surface [49], Fig. 9a.
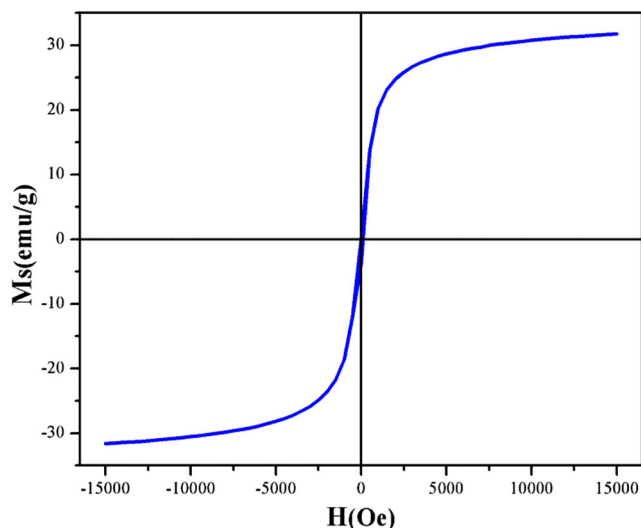

**Fig. 6** Room temperature magnetization curve of Fe_3O_4 NPs

3.2.2 Effect of pH

The degree of adsorption of CV on the surface of Fe_3O_4 NPs is critically dependent on pH of reaction mixture. In order to investigate effect of pH on dye removal, the dye solutions were prepared at different pH values between 4 and 12. Then adsorption of CV dye on Fe_3O_4 NPs was investigated at 50 mg, 200 min and 298 K of adsorbent dosage, contact time and temperature, respectively. It is found that the CV removal efficiency was increased with increase of pH of dye solution, Fig. 9b. The maximum dye removal efficiency was found at pH = 10, i.e., 93% of initial dye concentration (5 mg/L). Adsorption of CV dye on Fe_3O_4 NPs is ascribed to the electrostatic attractions between the negatively charged Fe_3O_4 NPs adsorbent and cationic CV dye. At high solution pH, cationic dye adsorption is preferable when compared to anionic dye adsorption [50].

3.2.3 Effect of adsorbent dosage on adsorption

In order to investigate the effect of adsorbent dosage on adsorption of dye, initial concentration of dye of 5 mg·L^{-1}, pH = 10 and temperature 298 K were maintained. The same experiment was carried out by varying the initial adsorbent concentration from 5, 15, 25, 50, and 100 mg, while all the other experimental parameters remains constant. The results (Fig. 9c) revealed that the dye removal efficiency was increased with increase of

Fig. 7 TGA and derivative TGA of Fe_3O_4 NPs
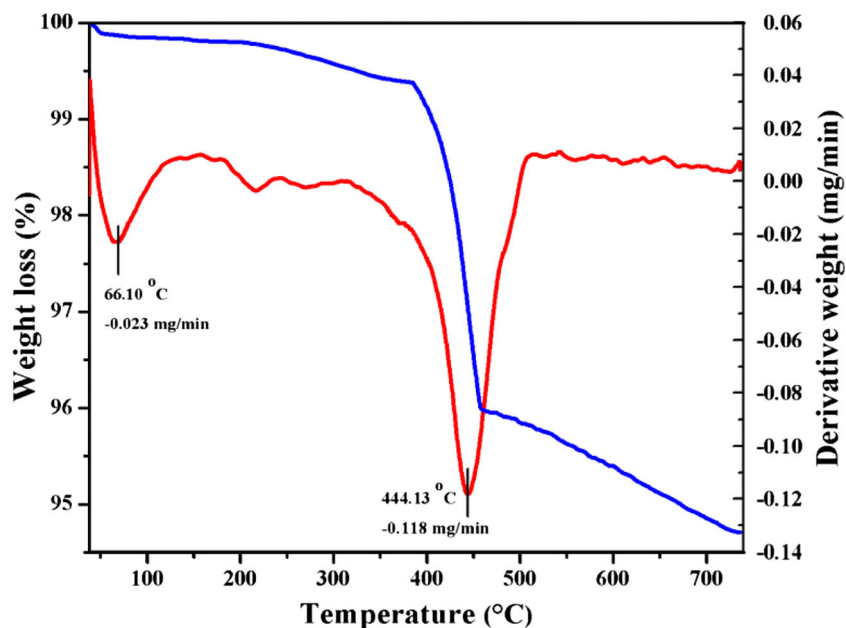
adsorbent dosage. This could be explained due to availability of more surface area, thereby leading to more binding sites for the adsorption of target CV dye onto the Fe_3O_4 NPs adsorbent.
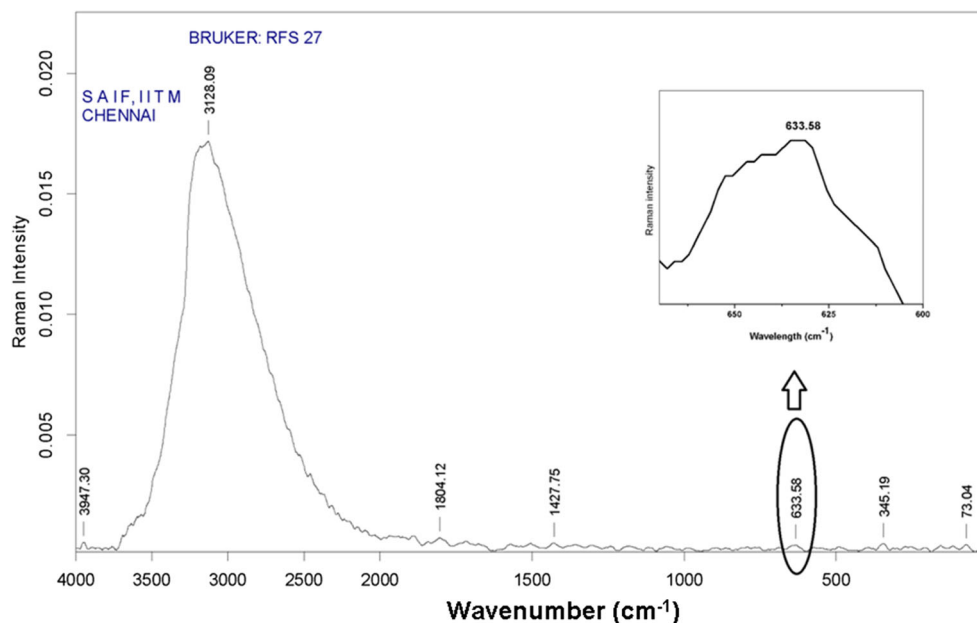
3.2.4 Effect of temperature

Temperature is one factor that seriously affects the dye removal efficiency. In order to investigate the effect of temperature on CV removal by Fe_3O_4 NPs, adsorption was carried out at 298, 308 and 318 K. The results clearly shows the adsorption percent decreased with increase of temperature, Fig. 9d. The decrease in

adsorption of dye with increase of temperature indicated exo-thermic nature of the adsorption process predominantly by vir-tue of reduction in Van der Waals forces between dye molecules and active sites on surface of Fe_3O_4 NPs [51].

3.3 Adsorption isotherms

Adsorption isotherms were employed to evaluate the perfor-mance of adsorbent for removal of CV from contaminated water. Quantitative data gathered was interpreted by using Langmuir, Freundlich and Temkin isotherms
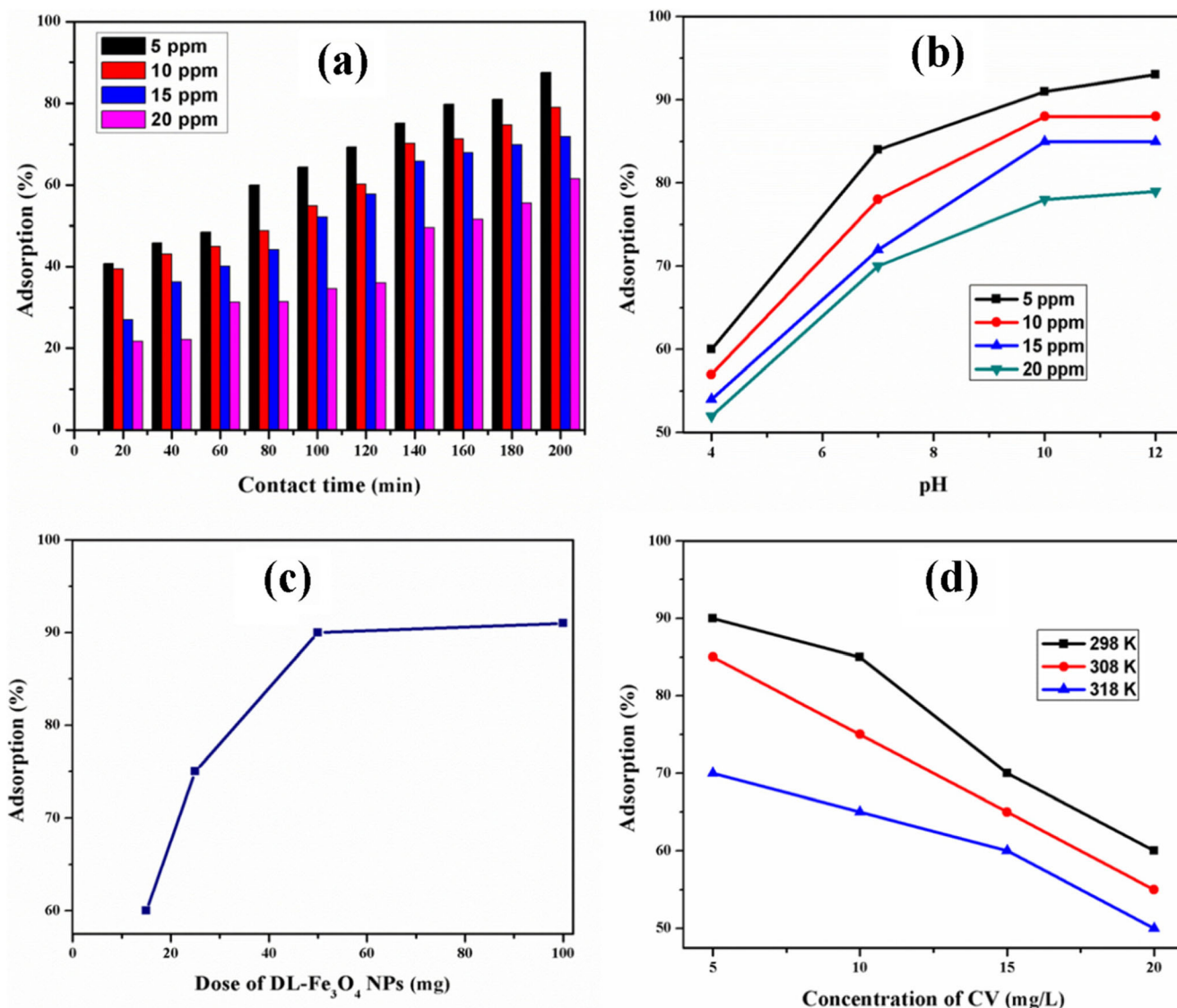
Fig. 8 FT-Raman spectra of Fe_3O_4 NPs

Fig. 9 Effect of percent of dye adsorption by Fe_3O_4 NPs at **a** initial concentration of CV dye, **b** pH of solution, **c** Dose of Fe_3O_4 NPs adsorbent and **d** Temperature

3.3.1 Langmuir isotherm

Langmuir adsorption isotherm is based on unilayer, uniform and finite adsorption sites on the surface of the adsorbent [52, 53]. When adsorption equilibrium is reached no further adsorption process takes place as well as adsorbed molecules along the same side will not have interaction to each other. Mathematically, tthe Langmuir isotherm is delineated as in equation 4.

$$C_e/q_e = 1/K_L q_{max} + C_e/q_{max} \qquad (4)$$

Where, 'Ce' is the equilibrium concentration of CV in the aqueous solution ($mg \cdot L^{-1}$), 'K_L' is the Langmuir equilibrium constant related to the enthalpy of the process ($L \cdot mol^{-1}$), q_{max}

is the maximum adsorption capacity of the adsorbent, i.e. Fe_3O_4 NPs ($mg \cdot g^{-1}$), and 'q_e' is the amount of CV adsorbed per dose of adsorbent at equilibrium ($mg \cdot g^{-1}$).

The Langmuir isotherm can also be expressed in terms of a dimensionless constant known as equilibrium parameter, Eq. 5.

$$R_L = 1/(1 + K_L C_o) \qquad (5)$$

Where, 'K_L' is the Langmuir constant and 'Co' is the highest initial concentration of the dye ($mg \cdot L^{-1}$). If ($0 < R_L < 1$) then adsorption is *favorable*; ($R_L = 1$) is *linear*; ($R_L > 1$) is *unfavorable* and ($R_L = 0$) is *irreversible*. In this particular study, R_L value was calculated to be 0.366 when Co = 5 mg/ L, indicates favorable dye adsorption.

3.3.2 Freundlich isotherm

Freundlich adsorption isotherm [54] is an empirical relation between the concentrations of a solute on the surface of an adsorbent to the concentration of the solute in the liquid with which it is in contact. This model assumed that the surface heterogeneity of the adsorbent as well as multilayer coverage on the surface. The linear equation of Freundlich isotherm is given as Eq. 6.

$$\log q_e = \log K_F + 1/n \log C_e \tag{6}$$

Where, 'q_e' is the amount of dye adsorbed per unit weight of adsorbent ($mg \cdot g^{-1}$), 'C_e' is the dye equilibrium concentration in solution ($mg \cdot L^{-1}$), 'K_F' is Freundlich constant indicative of the relative adsorption capacity of the adsorbent ($mg \cdot g^{-1}$) and 'n' is adsorption intensity in the Freundlich equation. In this study, the adsorption intensity 'n' value is greater than 1, implies that CV is favorably adsorbed on Fe_3O_4 NPs [55].

3.3.3 Temkin isotherm

Temkin adsorption isotherm [56] is applied to investigate the heat of adsorption and adsorbate-adsorbent interaction with the adsorbent surface. The model assumes that the heat of adsorption (function of temperature) of all molecules in the layer would decrease linearly rather than logarithmic with coverage. The linear equation of the Temkin isotherm is represented as Eq. 7.

$$q_e = B_1 \ln K_T + B_1 \ln C_e \tag{7}$$

Where, 'q_e' is equilibrium dye concentration on the adsorbent, 'B_1' is the Temkin adsorption constant related to the heat of sorption ($J \cdot mol^{-1}$) and 'K_T' is Temkin isotherm equilibrium binding constant ($L \cdot g^{-1}$) and 'C_e' equilibrium dye concentration in the solution ($mg \cdot L^{-1}$).

The adsorption isotherms analyzed by the three models for CV adsorption on Fe_3O_4 NPs are shown in Fig. 10, and all the parameters and R^2 values for the three models are included in Table S2†. The regression coefficients (R^2) obtained from Langmuir, Freundlich and Temkin models are 0.996, 0.985 and 0.991, respectively. Therefore, adsorption data are best fitted to Langmuir isotherm than Freundlich and Temkin isotherms and CV adsorption on the surface of Fe_3O_4 NPs is monolayer physical adsorption. The maximum monolayer adsorption. The monolayer adsorption maximum capacity (q_{max}) of CV on Fe_3O_4 NPs was found to be 56 $mg \cdot g^{-1}$ adsorbent by using 5 ppm initial concentrations of the CV at pH 10. Hayasi et al. [57] have reported adsorption capacity for CV using Poly(styrene-co-methacrylic acid) coated Fe_3O_4 NPs to be 416.66 mg/g adsorbent. At lower pH value, adsorption capacity was lower due to the similarity of charges between Fe_3O_4 NPs and CV i.e. cationic. However, with increase of pH of the dye solution, adsorption capacity also increased due to ionization of fatty acid methyl ester on the surface of Fe_3O_4 NPs and the negatively charged Fe_3O_4 NPs could attract cationic CV dye. Therefore, adsorption efficiency of Fe_3O_4 NPs was increased with increase of pH of dye solution.

3.4 Kinetic studies

The mechanism of adsorption mechanism is dependent on the physical and chemical properties of the adsorbents as well as mass transfer processes. In the present study, adsorption mechanism was investigated by fitting pseudo-first-order and pseudo-second-order reactions to the experimental data. The kinetics model parameters and constants of 5 $mg \cdot L^{-1}$ CV dye onto Fe_3O_4 NPs are shown in Table S3†. The Lagergren pseudo-first-order model [58] is given below as Eq. 8.

$$\ln(q_e - q_t) = \ln q_e - K_1 t \tag{8}$$

Where, 'q_e' and 'q_t' are the amount of the dye adsorbed at equilibrium and time, 't' in ($mg \cdot g^{-1}$), k_1 is rate constant of pseudo-first order kinetic model in (min^{-1}) and t is time in min. The pseudo-second-order kinetics [59] is expressed as in equation 9 below.

$$t/q_t = 1/k_2 q_e^2 + t/q_e \tag{9}$$

Where, 'k_2' is pseudo-second-order rate constant. Kinetic plots of adsorption of CV on Fe_3O_4 NPs using different initial dye concentrations for pseudo-first-order and pseudo-second-order using pH = 10 at 298 K is depicted in Fig. 11.

3.5 Adsorption thermodynamics

To study the effect of temperature on adsorption efficiency of Fe_3O_4 NPs with respect to CV, the initial concentration (5 ppm) and pH = 10 were kept constant and temperature was kept at 298 K, 308 K, and 318 K. With increasing temperature, adsorption capacity of Fe_3O_4 NPs was diminished. Adsorption of CV on the surface of Fe_3O_4 NPs is an exothermic process, i.e. heat is released to the environment. The energy changes associated with the adsorption process using the thermodynamic parameters were expressed by Eqs. 10 and 11.

$$\Delta G^\circ = \Delta H^\circ - T\Delta S^\circ \tag{10}$$

$$\ln K_{eq} = (\Delta S^\circ/R) - 1/T(\Delta H^\circ/R) \tag{11}$$

Where, '$\Delta G°$' is standard Gibbs free energy change, '$\Delta H°$' is change in enthalpy, '$\Delta S°$' is change in entropy, 'K_{eq}' is Langmuir isotherm constant related to Eq. 4, 'T' is temperature in K, and 'R' is general gas constant. The slope and Y-intercept from Van't Hoff plot ($\ln K_{eq}$ vs $1/T$) was used to calculate $\Delta H°$ and $\Delta S°$ of the adsorption process, Fig. 10d. The adsorption process is an exothermic since the adsorption
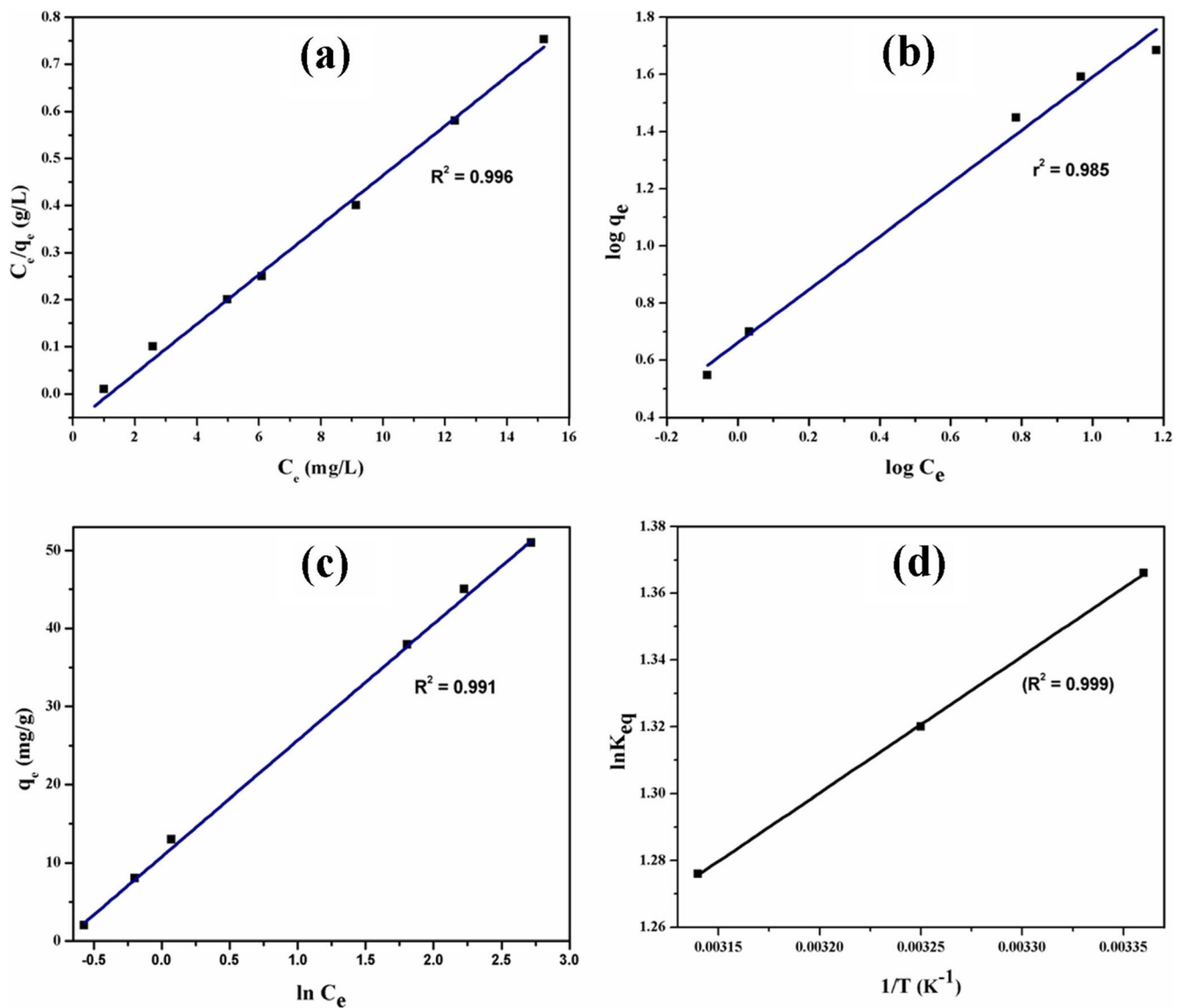
Fig. 10 Plots of **a** Langmuir isotherm, **b** Freundlich isotherm, **c** Temkin isotherm and **d** Thermodynamics of CV dye adsorption on Fe$_3$O$_4$ NPs sample
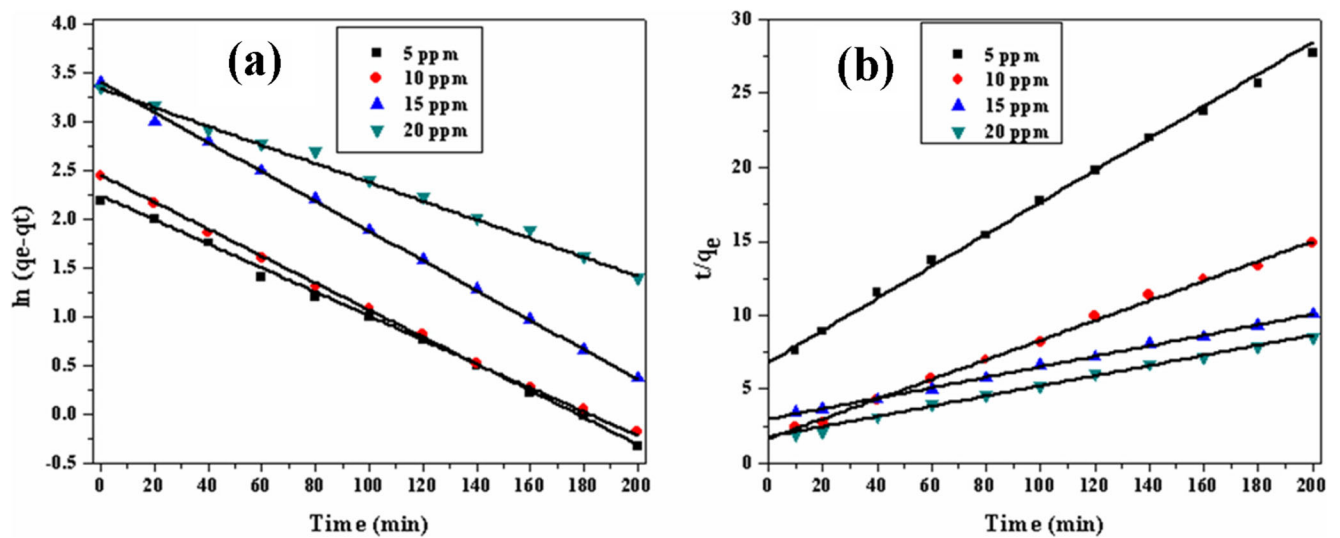

Fig. 11 Plots of adsorption of CV on Fe$_3$O$_4$ NPs at different dye concentrations **a** Pseudo-first-order kinetic model, **b** Pseudo-second-order kinetic model

capacity decreased with increase of temperature. The parameters of CV dye adsorption on Fe_3O_4 NPs are presented in Table S4†. Then negative value of '$\Delta G°$' implies that the spontaneous adsorption process while negative $\Delta H°$ and $\Delta S°$ values imply that the exothermic physical adsorption of CV dye molecules on Fe_3O_4 NPs.

3.6 Recyclability of adsorbent

The recyclability of Fe_3O_4 NPs for removal of CV was carried out five times. At the end of each reaction time, Fe_3O_4 NPs was collected by external magnet, washed with Milli-Q water and ethanol, and dried at 60 °C under vacuum for 12 h. The removal efficiency of CV dye after five cycles is found to be 84%, [Fig. 12].

4 Conclusion

Biomolecules capped magnetite nanoparticles were successfully synthesized using an aqueous pod extract of *Dolichos lablab* by co-precipitation method. UV-vis, FTIR and FT-Raman proved the synthesis of Fe_3O_4 NPs and capping and stabilization of Fe_3O_4 by biomolecules present in the plant extract. FE-SEM and TEM revealed the spherical shaped Fe_3O_4 NPs with particle size of 12.5 nm. The biomolecules capped Fe_3O_4 NPs very efficiently removed the CV present in the contaminated water. The adsorption process was best fitted to Langmuir adsorption model and follows the pseudo-second-order kinetics implies physical adsorption due to presence of cavities on the surface of Fe_3O_4 NPs. The adsorption efficiency of Fe_3O_4 NPs for CV dye was found to be 56 mg·g^{-1} at pH = 10.
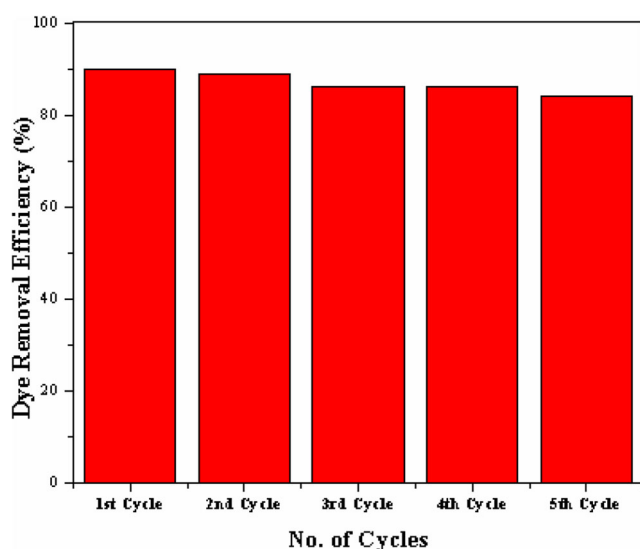
Fig. 12 The adsorption efficiency of Fe_3O_4 NPs after 5 cycles

Compliance with ethical standards

Conflict of interest The authors declare that they have no conflict of interest.

References

1. B.D. Terris, T. Thomson, J. Phys. D Appl. Phys. **38**, R199–R222 (2005)
2. K. Sun, C. Sun, S. Tang, CrystEngComm **18**, 641 (2016)
3. M. Franzreb, M. Siemann-Herzberg, T.J. Hobley, O.R.T. Thomas, Appl. Microbiol. Biotechnol. **70**, 505–516 (2006)
4. B.H. Kim, N. Lee, H. Kim, K. An, Y.I. Park, Y. Choi, K. Shin, Y. Lee, S.G. Kwon, H.B. Na, J.-G. Park, T.-Y. Ahn, Y.-W. Kim, W.K. Moon, S.H. Choi, T. Hyeon, J. Am. Chem. Soc. **133**, 12624 (2011)
5. R. Qiao, C. Yang, M. Gao, J. Mater. Chem. **19**, 6274 (2009)
6. U. Ikoba, H. Peng, H. Li, C. Miller, C. Yu, Q. Wang, Nanoscale **7**, 4291 (2015)
7. M.T. López-López, J.D.G. Durán, A.V. Delgado, F. González-Caballero, J. Colloid Interface Sci. **291**, 144 (2005)
8. A.L. Kavitha, H. Gurumallesh Prabu, S. Ananda Babu, S.K. Suja, J. Nanosci. Nanotechnol. **13**, 98–104 (2013)
9. Y.-W. Jun, Y.-M. Huh, J.-S. Choi, J.-H. Lee, H.-T. Song, S. Kim, S. Yoon, K.-S. Kim, J.-S. Shin, J.-S. Suh and J. Cheon, J. Am. Chem. Soc. **127**, 5732 (2005)
10. S. Sun, C.B. Murray, D. Weller, L. Folks, A. Moser, Science **287**, 1989 (2000)
11. M.M. Miller, G.A. Prinz, S.-F. Cheng, S. Bounnak, Appl. Phys. Lett. **81**, 2211–2213 (2002)
12. N. Basavegowda, K. B. S. Magar, K. Mishra, Y. R. Lee, New J. Chem. **38**, 5415 (2014)
13. I. Ali, C. Peng, I. Naz, Z.M. Khan, M. Sultan, T. Islam, I.A. Abbasi, RSC Adv. **7**, 40158 (2017)
14. W. Rongcheng, Q. Jiuhui, Water Environ. Res. **76**, 2637 (2004)
15. S. Gao, Y. Shi, S. Zhang, K. Jiang, S. Yang, Z. Li, E. Takayama-Muromachi, J. Phys. Chem. C **112**, 10398 (2008)
16. W. Zhang, F. Shen, R. Hong, Particuology **9**, 179 (2011)
17. K. Nakatsuka, B. Jeyadevan, S. Neveu, H. Koganezawa, J. Magn. Magn. Mater. **252**, 360–362 (2002)
18. B.M. Kumfer, K. Shinoda, B. Jeyadevan, I.M. Kennedy, J. Aerosol Sci. **41**, 257 (2010)
19. O.M. Lemine, K. Omri, B. Zhang, L. El Mir, M. Sajieddine, A. Alyamani, M. Bououdina, Superlattices Microst. **52**, 793 (2012)
20. F. Fajaroh, H. Setyawan, W. Widiyastuti, S. Winardi, Adv. Powder Technol. **23**, 273 (2012)
21. J.F. de Carvalho, S.N. de Medeiros, M.A. Morales, A.L. Dantas, A.S. Carriço, Appl. Surf. Sci. **275**, 84–87 (2013)
22. R. Vijayakumar, Y. Koltypin, I. Felner, A. Gedanken, Mater. Sci. Eng. A **286**, 101 (2000)
23. Y. Hou, H. Kondoh, M. Shimojo, T. Kogure, T. Ohta, J. Phys. Chem. B **109**, 19094 (2005)
24. K. Mondal, H. Lorethova, E. Hippo, T. Wiltowski, S.B. Lalvani, Fuel Process. Technol. **86**, 33 (2004)
25. P. Jian, H. Yahui, W. Yang, L. Linlin, J. Memb. Sci. **284**, 9–16 (2006)

26. K.N. Thakkar, S.S. Mhatre, R.Y. Parikh, Nanomedicine **6**, 257 (2010)

27. M. Mahdavi, F. Namvar, M. Ahmad, R. Mohamad, Molecules **18**, 5954 (2013)

28. P. Mohanpuria, N.K. Rana, S.K. Yadav, J. Nanopart. Res. **10**, 507 (2007)

29. Abhilash, K. Revati and B. D. Pandey, Bull. Mater. Sci. **34**, 191 (2011)

30. W. Jiang, K. Lai, K. Liu, R. Xia, F. Gao, Y. Wu, Z. Gu, Nanoscale **6**, 1305 (2014)

31. A. Kumar Das, A.K. Das, A. Marwal, R. Verma, Nano Hybrids **7**, 69 (2014)

32. A. M. Awwad and N. M. Salem, Nanosci. Nanotechnol. Lett. **2**, 125 (2013)

33. Y. Cai, Y. Shen, A. Xie, S. Li, X. Wang, J. Magn. Magn. Mater. **322**, 2938–2943 (2010)

34. S.P. Rajendran, K. Sengodan, J. Nanosci. Nanotechnol., **2017** (2017)

35. V. C. Karade, P. P. Waifalkar, T. D. Dongle, Subasa C. Sahoo, P. Kollu, P. S. Patil, P. B. Patil, Mater. Res. Express **4**, 096102 (2017)

36. A.L. Ramirez-Nuñez, L.F. Jimenez-Garcia, G.F. Goya, B. Sanz, J. Santoyo-Salazar, Nanotechnology **29**, 074001 (2018)

37. V.V. Makarov, S.S. Makarova, A.J. Love, O.V. Sinitsyana, A.O. Dudnik, I.V. Yaminsky, M.E. Taliansky, N.O. Kalinina, Langmuir **30**, 5982 (2014)

38. E.C. Njagi, H. Huang, L. Stafford, H. Genuino, H.M. Galindo, J.B. Collins, G.E. Hoag, S.L. Suib, Langmuir **27**, 264 (2011)

39. S.F. Hasany, S.F. Hasany, I. Ahmed, J. Rajan, A. Rehman, Nanosci. Nanotechnol. Lett. **2**, 148 (2013)

40. A.A. Fernandes, G. Nagendrappa, J. Agric. Food Chem. **27**, 795 (1979)

41. N. Belachew, D. Rama Devi, K. Basavaiah, J. Exp. Nanosci. **12**, 114–128 (2017)

42. R.K. Sharma, S. Dutta, S. Sharma, R. Zboril, R.S. Varma, M.B. Gawande, Green Chem. **18**, 3184 (2016)

43. A.M. Atta, G.A. El-Mahdy, H.A. Al-Lohedan, S.A. Al-Hussain, Int. J. Mol. Sci. **15**, 6974–6989 (2014)

44. F. Buazar, M.H. Baghlani-Nejazd, M. Badri, M. Kashisaz, A. Khaledi-Nasab, F. Kroushawi, Starch-Stärke **68**, 796 (2016)

45. R.M. Cornell, U. Schwertmann, *The Iron Oxides: Structure, Properties, Reactions, Occurrences and Uses*. (Wiley, 2006)

46. Z. Wang, M. Lu, RSC Adv. **1234** (2014)

47. F. Ador, Spectroscopy **31**, 22–27 (2016)

48. L. Ying-Sing, J.S. Church, A.L. Woodhead, J. Magn. Magn. Mater. **324**, 1546 (2012)

49. Z. Eren, F.N. Acar, Desalination **194**, 1 (2006)

50. M. A. M. Salleh, D. K. Mahmoud, W. A. W. Abdul Karim, A. Idris. Desalination **280**, 1 (2011)

51. A. Ofomaja, Y. Ho, Dyes Pigments **74**, 60 (2007)

52. Y.C. Sharma, A.S.K.S. Uma, S.N. Upadhyay, J. Chem. Eng. Data **55**, 5777 (2010)

53. I. Langmuir, J. Franklin Inst. **183**, 102 (1917)

54. H. Freundlich, Z. Phys. Chem. **57**, 385. https://doi.org/10.1515/zpch-1907-5723

55. N. Mohammadi, H. Khani, V.K. Gupta, E. Amereh, S. Agarwal, J. Colloid Interface Sci. **362**, 457 (2011)

56. M.I. Tempkin, V. Pyzhev, Acta Phys **12**, 327 (1940)

57. M. Hayasi, M. Karimi, Polym. Bull. **74**, 1995–2016 (2016)

58. S. Y. Lagergren, Zur Theorie der sogenannten Adsorption gelöster Stoffe, 24, 1–39 (1898)

59. D. Robati, J Nanostruct Chem **3**, 55 (2013)